Available online at www.sciencedirect.com
SCIENCE DIRECT®
Polymer 45 (2004) 3671–3679
polymer
www.elsevier.com/locate/polymer

Phase behavior of semicrystalline polymer blends

Chieh-Tsung Lo[a], Soenke Seifert[b], Pappannan Thiyagarajan[c], Balaji Narasimhan[a,*]

[a]*Department of Chemical Engineering, Iowa State University, 2035 Sweeney Hall, Ames, IA 50011-2230, USA*
[b]*Advanced Photon Source, Argonne National Laboratory, 9700 S. Cass Avenue, Argonne, IL 60439 USA*
[c]*Intense Pulsed Neutron Source, Argonne National Laboratory, 9700 S. Cass Avenue, Argonne, IL 60439 USA*

Received 31 October 2003; received in revised form 18 March 2004; accepted 29 March 2004

Abstract

The phase behavior of the semicrystalline polymer blend composed of isotactic polypropylene (iPP) and linear low density polyethylene (PE) was studied using small angle X-ray scattering (SAXS) and optical microscopy (OM). Based on the random phase approximation, the iPP/PE interaction parameter, χ, was obtained, and used to construct the iPP/PE phase diagram. The χ values reported in this study are lower than the χ values for deuterium-labeled moieties, measured by small angle neutron scattering (SANS). The predicted phase diagram has upper critical solution temperature (UCST) behavior with a critical temperature of 143 °C for the molecular weights used in this study. OM was used to locate cloud points and the results are consistent with the predicted phase diagram. Since iPP melts above the critical point, care was taken to distinguish phase separation from iPP crystallization by studying the kinetics of iPP crystallization, and the iPP crystallization was discerned from dewetting. In PE-rich blends, the iPP crystallization was suppressed and no dewetting was observed.

Keywords: Semicrystalline polymers; SAXS; Phase behavior

1. Introduction

Polymer blends have received much attention for many decades. The properties of polymer blends (such as mechanical strength, surface bonding, and resistance) are a strong function of the blend morphology. This morphology and the associated phase behavior strongly depend on the miscibility between the components of the blend. Thus, a fundamental understanding of the miscibility of the components in the blend is crucial for end applications. Other factors that decide if the system is in one phase or in multiple phases include polymer molecular weight, blend composition, and species with specific chemical or physical interactions with each other. In semicrystalline polymers, the phase behavior is even more complicated since these polymers crystallize between their glass transition and melting temperatures. Both liquid–solid demixing due to crystallization and liquid-liquid phase separation play an important role on the end use. The final properties will strongly depend on crystallinity, phase morphology, and the interfacial adhesion.

Much research has been focused on the semicrystalline polymer blend system, isotactic polypropylene/polyethylene (iPP/PE), and studies focused on the phase morphology and related mechanical properties have been performed. The compatibility of the iPP/PE system is quite different depending on the type of PE chain structure utilized in the study. With flexible PE of small molecular weight, the iPP/PE blend is miscible due to the increased combinatorial entropy. It has been reported that iPP is miscible with LLDPE in blends with iPP content less than 20% [1]. In addition, as the system is annealed, instead of forming droplets as with HDPE and LDPE [2,3], co-crystallization occurs in the iPP/LLDPE system [4,5], and iPP crystallizes as an open arm structure [2,3]. The crystallization rate of iPP also decreases for two reasons. The first is that iPP in PE can be viewed as iPP in solution [2,3,5], and the iPP nucleation is reduced. The second is that the viscous LLDPE slows the diffusion of iPP chains during crystallization [3]. In iPP/HDPE blends, no co-crystallization occurs [6,7], and HDPE delays the nucleation and crystallization rate of iPP [8]. In this system, the lamellar thickness of iPP is dependent on the blend composition [9]. In PP/LDPE system, Dong et al. [10] reported miscibility when the iPP content is below 15%, but Teh [11] argued that since PE and

* Corresponding author. Tel.: +1-515-294-8019; fax: +1-515-294-2689.
E-mail address: nbalaji@iastate.edu (B. Narasimhan).

0032-3861/$ - see front matter © 2004 Published by Elsevier Ltd.
doi:10.1016/j.polymer.2004.03.089

iPP crystallize in orthorhombic and monoclinic α form, respectively, which are not miscible, the system is immiscible. Irrespective of the type of PE used in the study, the mechanical properties have a nonlinear relationship with blend composition [12–17], and LLDPE/iPP blends have superior mechanical properties [18] due to the greater miscibility of the polymers. In this work, we present an experimental study using synchrotron small angle X-ray scattering (SAXS) and optical microscopy (OM) of the phase behavior of the polyolefin blend system composed of iPP and linear low density polyethylene (PE). This work has important implications for strengthening interfaces between these semicrystalline polymers, which will be the subject of a future publication.

1.1. Theoretical background

The miscibility of binary polymer mixtures can be predicted from the free energy of mixing by the Flory–Huggins theory [19]:

$$\frac{\Delta G_m}{RT} = \frac{\phi_A}{N_A}\ln\phi_A + \frac{\phi_B}{N_B}\ln\phi_B + \chi\phi_A\phi_B \quad (1)$$

Here χ is the Flory–Huggins interaction parameter, ϕ_i is the volume fraction and N_i is the degree of polymerization of species i, and T is the temperature. In Eq. (1), the first two terms on the right hand side are entropic contributions, while the third term is enthalpic in nature, and is derived from:

$$\chi = \frac{\Delta H_m}{RTN_A\phi_B} \quad (2)$$

In polymer systems, since N_A and N_B are large, the magnitude of the entropy term is usually small, so χ, which is in the enthalpic term, determines the phase behavior of the system.

If the system is miscible, the free energy of mixing must obey the conditions in Eqs. (3) and (4).

$$\Delta G_m < 0 \quad (3)$$

$$\left(\frac{\partial^2\Delta G_m}{\partial\phi_A^2}\right)_{T,P} > 0 \quad (4)$$

In Eq. (1), the entropic term is always negative, so if χ is negative, the system is usually miscible based on Eq. (3), but it may still be phase separated due to the limits imposed by Eq. (4).

In general, χ is a function of both temperature and blend composition [20,21]. Many scattering studies reveal a weak composition dependence of χ (Lin et al. [22]). Thus, in this study χ is only a function of temperature as shown in Eq. (5) [23].

$$\chi = A + \frac{B}{T} \quad (5)$$

1.2. Experimental measurements of χ in polyolefin blends

A large body of literature exists on the interaction parameter of polyolefin blends by small angle neutron scattering (SANS) [22,24–28] and molecular modeling [23,29–32]. However, to our knowledge, there is no report in the literature of using SAXS to measure χ and predict the phase diagram of iPP/PE blend system. The use of SAXS is important since SANS requires deuterium substitution to provide neutron scattering contrast, while SAXS exploits electron density differences, present in the iPP/PE system. Furthermore, the difference in the bond length and polarizability of hydrogenated (C–H) and deuterated (C–D) bonds make it difficult to relate the SANS results to the unlabeled system. Graessley et al. [28] use a solubility parameter-based argument to show that the interaction parameter in the unlabeled system can be estimated as

$$\chi_{hh} = \left(\frac{\chi_{hd}^{1/2} + \chi_{dh}^{1/2}}{2}\right)^2 \quad (6)$$

Here χ_{hh} is the value of χ when neither species contain deuterium, and χ_{dh} and χ_{hd} are the values of χ when each component is, respectively, labeled by deuterium. Usually, the values of χ_{dh} and χ_{hd} are quite different, and the difference decreases slightly with increasing temperature. It has been shown that χ_{dh} or χ_{hd} is larger when the more branched component is labeled due to the creation of greater long-chain interaction [24]. Eq. (6) can be further simplified to Eq. (7) [22,28].

$$\chi_{hh} = \frac{\chi_{dh} + \chi_{hd}}{2} \quad (7)$$

Further, it has been reported that for some polyolefins, the critical temperature of the unlabeled blends is the arithmetic mean of the critical temperature of the singly labeled blends [24]. The data of Jeon et al. on mixtures of labeled and unlabeled polyolefins do not agree with Eqs. (6) and (7) or with the critical temperature prediction reported in Ref. [28]. Thus, it is apparent that the thermodynamic effects of deuterium labeling are poorly understood. Hence, in this work, we have used SAXS to measure the temperature dependent interaction parameter in the semicrystalline iPP/PE blend system, and verified the phase diagram by optical microscopy. The idea is to obtain reliable iPP/PE interaction parameters from SAXS, without having to account for the effect of deuterium. The results will be compared with the χ values obtained from SANS studies.

2. Experimental section

2.1. Materials

Isotactic polypropylene (Achieve™ 3854) and linear low density polyethylene (Exceed™ mLLDPE) were provided

by Exxon Mobil. The properties of the materials are shown in Table 1. Both the melting temperature and the degree of crystallinity were measured by differential scanning calorimetry (DSC) (Perkin Elmer DSC-7, Shelton, CT) with a heating rate of 10 °C/min, and the molecular weight was measured using rheometry (ARES, Rheometrics, Piscataway, NJ). PE and iPP pellets of appropriate compositions were ground in a freezer mill (SPEX, CertiPrep 6756, NJ) and cooled by liquid nitrogen for 10 min. The well-mixed powders were used to make blends.

2.2. Synchrotron small angle X-ray scattering (SAXS)

Blends (50/50 (v/v)) for SAXS was prepared in DSC aluminum sample pans (Perkin Elmer, Shelton, CT) at 190 °C on a hot stage (A200, Fryer, IL) and sealed in the melt. The sample thickness (~1 mm) was accurately measured using a depth micrometer.

The SAXS experiments were performed at the Sector 12 ID at Argonne National Laboratory. The measurements were performed in situ with a cartridge heater at temperatures above the melting temperatures of two species in order to eliminate any crystallization. At steady state, five images were taken with a CCD detector with an exposure time of 0.5 s, and the images were averaged at each temperature. The sample to detector distance was 4 m and the X-ray energy was 12 keV. The data have been placed on an absolute intensity using the known scattering cross-section of a standard polyethylene sample.

2.2.1. Optical microscopy (OM)

The images of phase behavior with temperature dependence were studied by optical microscopy (Nikon, Eclipse ME 600L, JP) in the reflected mode. Samples were prepared by pressing the mixed iPP/PE powders at 190 °C for 30 min between cover slips with the film thickness of ~1 μm, which was pressed under a load of 100 pounds by a Carver Press (Wabash, IN). In situ experiments were performed on the Fryer hot stage and images were taken by a CCD camera (KP-M2, Hitachi, JP).

3. Results and discussion

3.1. Synchrotron SAXS

In the synchrotron SAXS study, the temperatures of interest are above the melting temperatures of the two materials (see Table 1). At these temperatures, the crystals of both polymers are eliminated, and the samples are in the amorphous phase. Since the temperatures of interest are higher than the melting temperatures, the blends were sealed in DSC aluminum sample pans to prevent materials from leaking out. Data were corrected by scattering from empty sample pan.

The scattering intensity from the microvoids in the blend [33] dominates in the very low q region ($I(q) \sim q^{-4}$) and the scattering from the polymers ($I(q) \sim q^{-2}$) occurs at $q > 0.01$ Å^{-1}. Here the scattering vector q is given by $4\pi \times \sin(\theta/2)/\lambda$, where θ is the scattering angle and λ is the wavelength of the incident X-rays. Hence, it is possible to subtract the scattering from the voids from the whole scattering data using the Porod law (Eq. (8)). One criterion to ascertain the adequacy of this procedure is to assure that the Debye region of the scattering from the polymers, that describes the random coil behavior of polymer molecules, becomes a horizontal line in the Kratky–Porod plot (q vs. Iq^2, not shown), and at higher q, the Kratky–Porod plot becomes a straight line that can be extrapolated to the origin [34].

$$I_p = \frac{K_p}{q^4} \tag{8}$$

Fig. 1(a) shows the absolute scattering intensity $I(q)$ for the polymer melt at different temperatures after the subtraction of the scattering from the sample pan and microvoids. The structure factor $S(q)$ is calculated from the absolute intensity [34,35]:

$$S(q) = \frac{I(q)}{(\Delta\rho)^2 V_s} \tag{9}$$

Here, $\Delta\rho$ is the electron density difference between two polymers and V_s is the lattice volume or the volume of monomer. In this study, we chose V_s as the iPP monomer volume.

From de Gennes' random phase approximation (RPA) theory [36], as q approaches zero, χ can be calculated from the intercept of the Zimm plot (S^{-1} vs. q^2) [37] as shown in Fig. 1(b).

$$S^{-1}(q \to 0) = 2(\chi_c - \chi) + \frac{2}{3}\chi_c R_\phi^2 q^2 \tag{10}$$

Here R_ϕ is the mean square radius of gyration of the two

Table 1
Molecular properties of iPP and PE used in this study

	M_n (g/mol)	Polydispersity index (PDI)	Melting temperature (°C)	Degree of crystallinity (W_c) (%)	Density (g/cm^3)
iPP	47,500	3.2	153	48	0.872
PE	32,400	3.1	117	26	0.912

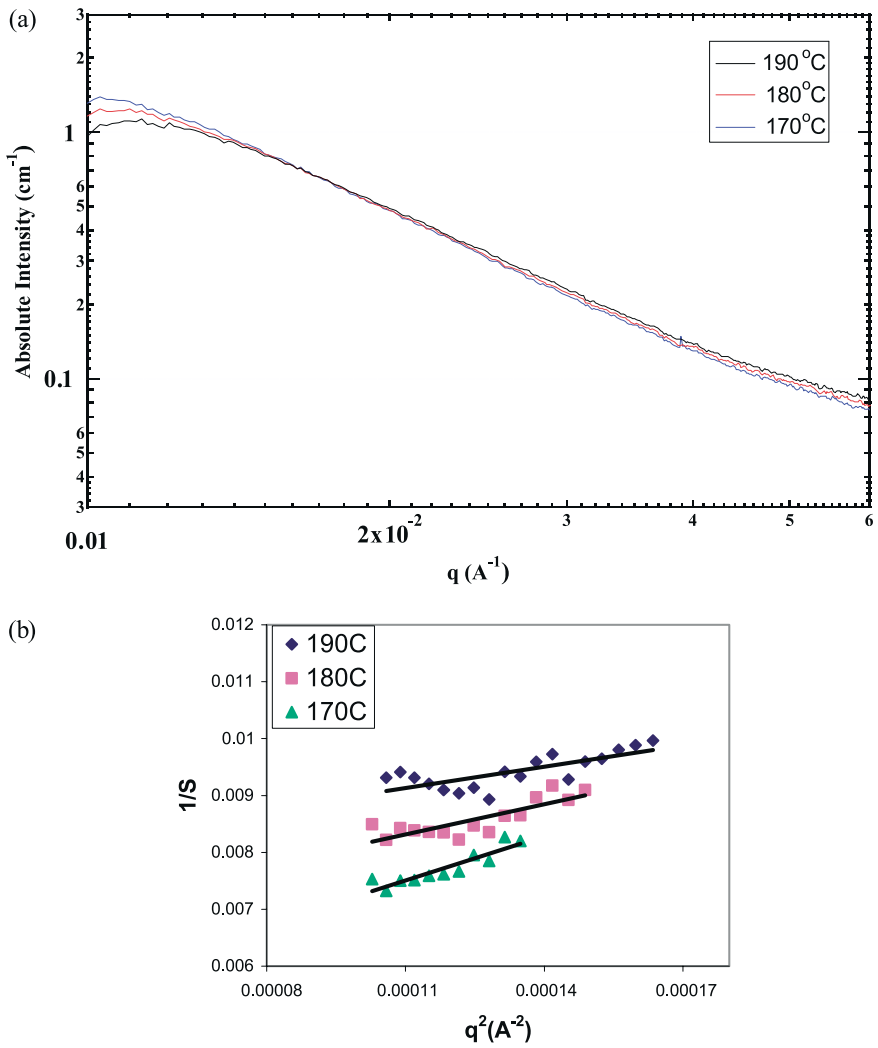

Fig. 1. (a) Absolute SAXS data of iPP/PE blends as a function of temperature after the subtraction of the scattering due to the aluminum pan and the microvoids, and (b) Zimm plot of the same $[1/S(q \to 0)$ vs. $q^2]$.

components, and is given by [37]:

$$R_\phi^2 = (1 - \phi_A)R_A^2 + \phi_A R_B^2 \tag{11}$$

R_ϕ can be obtained from the slope of Zimm plot once χ_c is known.

$$\frac{dS^{-1}(q \to 0)}{dq^2} = \frac{2}{3}\chi_c R_\phi^2 \tag{12}$$

χ_c is the value of χ at the critical point and can be derived by setting the second derivative of free energy of mixing to zero. This result is shown in Eq. (13). In our system, N_{iPP} and N_{PE} are 1131 and 1157, respectively, and χ_c calculated by Eq. (13) is 1.74×10^{-3}.

$$\chi_c = \frac{1}{2}\left[\frac{1}{N_A\phi_{A,c}} + \frac{1}{N_B(1 - \phi_{A,c})}\right] \tag{13}$$

Fig. 2 shows χ values from synchrotron SAXS at different temperatures, and Eq. (14) shows the variation of χ with temperature:

$$\chi = -0.0367 + \frac{16.01}{T} \tag{14}$$

In Fig. 2, χ decreases with increase in absolute temperature, indicating that the phase diagram of iPP/PE blends exhibits upper critical solution temperature (UCST) behavior. This result is consistent with phase diagrams reported in the literature [24] based on SANS measurements and with results predicted by lattice cluster theory (LCT) [23].

Table 2 compares the χ values obtained in this study with literature values [23,24]. In both SAXS and SANS, the entropic term (A in Eq. (5)) in the temperature dependence of χ is much smaller than that in the LCT, but enthalpic term (B in Eq. (5)) is much larger. In the LCT, it was assumed that the interaction energy change, $\Delta\varepsilon$, which is the interaction involving atoms which are remote in the chain sequence (also called long chain interaction), is zero and the focus is on short chain interactions. From the internal energy

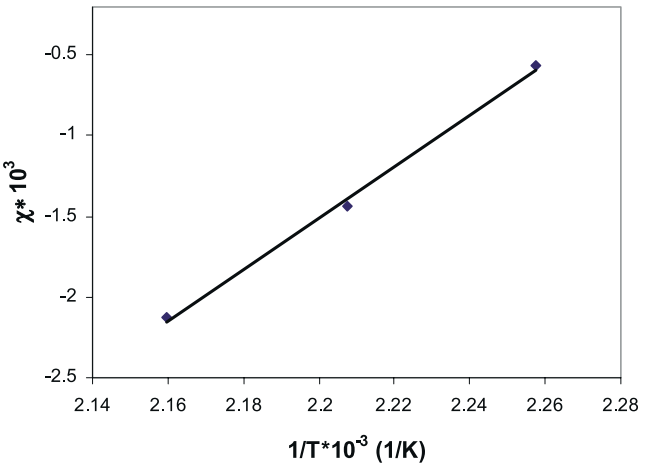

Fig. 2. Temperature dependence of χ from SAXS.

of mixing,

$$\Delta E_m = \Delta\epsilon N_A \phi_B \quad (15)$$

If the volume of mixing is neglected, the enthalpy of mixing can be written as:

$$\Delta H_m = \Delta E_m + P\Delta V_m = \Delta E_m = \Delta\epsilon N_A \phi_B \quad (16)$$

The free energy of mixing is

$$\Delta G_m = \Delta H_m - T\Delta S_m = \Delta\epsilon N_A \phi_B - T\Delta S_m \quad (17)$$

In incompatible, multicomponent systems, $\Delta\epsilon > 0$. However, LCT underestimates the value of $\Delta\epsilon$, thus making ΔG_m smaller, which favors miscibility. Thus, the interaction parameter χ is lower compared to the experimentally determined values from scattering data. Comparing the χ obtained from synchrotron SAXS and SANS [24], we observe that the entropic and enthalpic terms are of the same order of magnitude, but the A and B values in SANS are slightly higher than that in SAXS. As for SANS, due to the lack of neutron scattering contrast, deuterium substitution on one polymer is needed. Instead of merely having of hA/hB interactions in the unlabeled system, where A and B are the blend components and h represents the unlabeled components, deuterium labeling creates additional repulsive interactions between hA/dA and hB/dA if component A is labeled and between hA/dB and hB/dB is component B is labeled. This makes the system more incompatible, and the interaction parameter at the same temperature would be higher. Indeed, comparing χ values evaluated at 160 °C using the SAXS and SANS χ values shown in Table 2, we obtain $\chi_{hPE/hPP} = 0.0003$, $\chi_{hPE/dPP} = 0.0129$, and $\chi_{hPP/dPE} = 0.0095$. Jeon et al. [24] showed the effects of deuterium on homopolymer matched pairs, and χ of hPE/dPE and hPP/dPP mixtures are $1.34\times10^{-4} + 2.64/T$ and $-3.63\times10^{-3} + 1.64/T$, respectively, but there is still a small difference in the entropic term between SAXS and SANS after subtraction due to the deuterium effect on the homopolymers. The difference may also be due to the different chemical structure of polyethylene in the two studies. Also noteworthy is that the χ obtained in this study is not the arithmetic mean of the χ values with one labeled component. This is not surprising since the results shown in Eqs. (6) and (7) were derived by using solubility parameters, which are less accurate.

Table 2
Comparison of χ measured from SAXS with that from SANS [24] and LCT [23].

Method	χ	N
SAXS (this study)	$\chi = -0.0367 + 16.01/T$	$N_{iPP} = 1131$ $N_{PE} = 1157$
SANS (Jeon et al.) [24]	$\chi = -0.0276 + 17.56/T$ ($\chi_{hPE/dPP}$) $\chi = -0.0311 + 17.60/T$ ($\chi_{dPE/hPP}$)	$N_{iPP} = 178$ $N_{PE} = 83$
LCT (Freed et al.) [23]	$\chi = 0.001356 + 0.515/T$	$N_{iPP} = 18$ $N_{PE} = 27$

The iPP/PE phase diagram can be predicted by substituting χ in Eq. (1). The binodal curve is the locus of the points of co-tangency on isotherms in the $\Delta G_m/RT$ vs. ϕ curves. The spinodal curve can be obtained by setting the second derivative of the free energy of mixing to zero. The predicted phase diagram is shown in Fig. 3. The critical point obtained from this phase diagram is 143 °C.

The average radius of gyration (R_ϕ) of the *i*PP/PE blend calculated from Eq. (12) varies linearly from 10.2 to 14.8 nm over the range of temperature studied and exhibits a negative thermal coefficient of expansion. These values are slightly larger than literature values from SANS experiments [24]. In scattering experiments, the radius of gyration obtained is the *z*-average R_ϕ [38], and the value obtained is consistent with the polydispersity of our materials. The radius of gyration also decreases with increasing temperature. This result can be explained by considering that the ratio of trans to gauche conformations decreases with increase in temperature, as noted by previous researchers [39,40]. The number of trans sequences is large at low

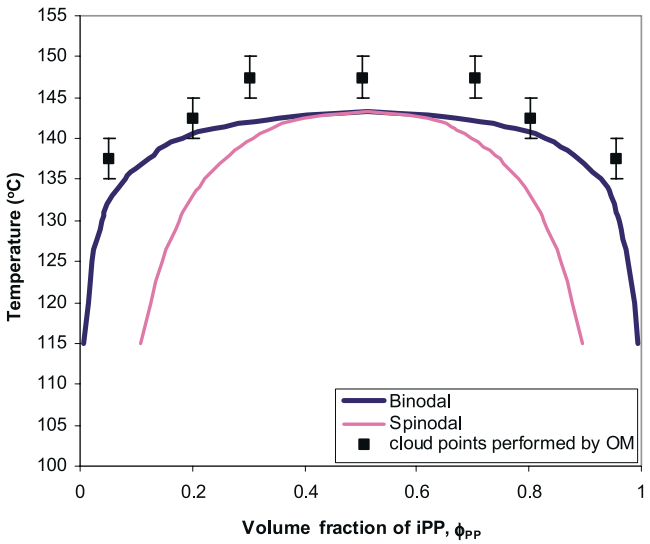

Fig. 3. Phase diagram predicted from SAXS and comparison with cloud points determined using optical microscopy.

temperature since it is the conformation with the lowest potential energy and as gauche sequences are added, the curvature of the chain increases, leading to a decrease in the radius of gyration with increasing temperature.

3.1.1. Optical microscopy

In this study, in situ optical microscopy was used to verify the phase diagram predicted from SAXS. Different compositions of iPP/PE blends were first melted at 170 °C for 30 min to eliminate the crystals. At this temperature, iPP and PE exhibit single phase behavior (see previous section). After 30 min, the temperature was quenched to the temperature of interest, and after equilibrium was reached, the images were recorded. In order to ensure that the system is at equilibrium, at each temperature, the blends were annealed for at least 3 h. The temperature was decreased from 170 °C by intervals of 5 °C. Using this procedure, cloud points can be obtained, and the phase diagram is shown in Fig. 3. The phase diagram obtained from optical microscopy agrees well with that predicted from SAXS. The small discrepancy between the observed cloud points and the phase boundary predicted by SAXS can be explained by considering the thermal resistance due to variable contact between the hot stage and the sample and the temperature fluctuation of the hot stage.

When looking for cloud points below the melting temperature of iPP, it is possible that iPP crystallites are present and these can lead to misinterpretation of the cloud point. This is because, during annealing, iPP crystallizes, and the growth of the iPP spherulites may resemble the droplets induced by liquid–liquid phase separation. This effect is more pronounced in blends with low PE compositions. In order to ascertain the differences between crystallization and phase separation, we studied both iPP homopolymer crystallization and iPP/PE blend crystallization. Fig. 4 shows OM images of iPP homopolymer annealed at 130 °C. We observe that iPP spherulites appear at 1 min (Fig. 4(a)), and the spherulite growth rate is fast. After 3 min (Fig. 4(b)), the individual growing spherulites start encountering each other, and impinge. This impingement erases the boundary of the spherulites, and causes the dewetting of iPP due to the appearance of crystals as shown in Fig. 4(c). After 10 min, equilibrium is reached, showing the totally dewetted iPP (Fig. 4(d)). We also used optical microscopy with polarized light to confirm the dewetting caused by crystallization and observed that dewetting only

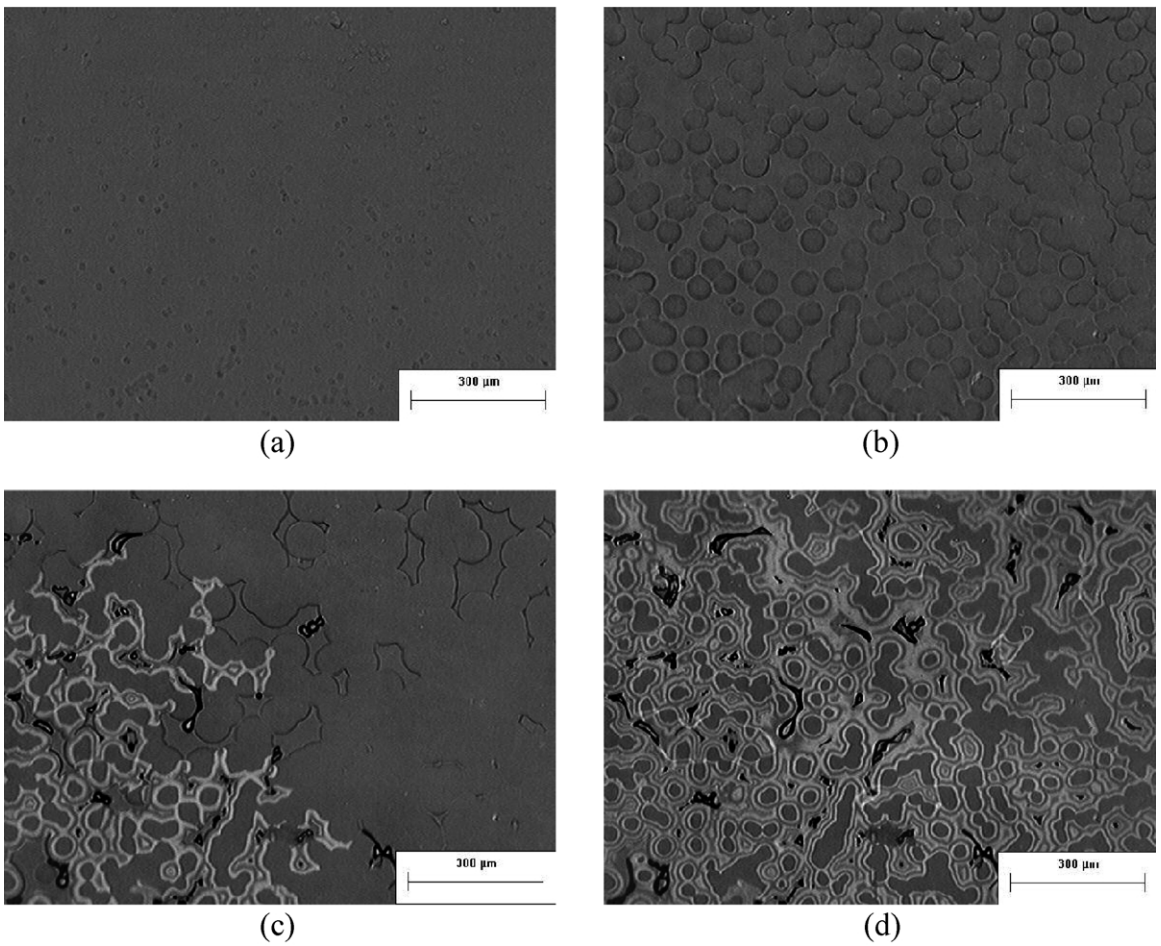

Fig. 4. The mechanism of iPP crystallization. The sample was annealed at 130 °C for: (a) 1 min, (b) 3 min, (c) 5 min, and (d) 10 min.

occurs in the spherulitic region, and does not exist in the amorphous region (data not shown).

Fig. 5 shows OM images of a 90/10 (v/v) iPP/PE blend annealed at 130 °C. The spherulite growth rate is much slower in this case than in the iPP homopolymer (see Fig. 4). After 3 min of annealing, small spherulites can be seen as shown in Fig. 5(a). The spherulites grow slowly and impinge after 30 min (Fig. 5(b) and (c)). As expected, the number of spherulites in the blend is much less than the number in the iPP homopolymer; additionally, the radius of the spherulites is larger. The iPP spherulite growth rate decreases with increasing PE content because PE dilutes the nucleation of iPP [1,3]. This behavior is more apparent in blends with high PE content and even after 3 h of annealing, the iPP spherulites are barely seen (data not shown). Dewetting due to iPP crystallization in the blend is shown in Fig. 5(d). In the blends, the wetting nature of PE decreases the area of dewetting available as compared to the case of iPP homopolymer. Thus, the small droplets in the images shown in Fig. 5(c) and (d) are due to liquid–liquid phase separation, which is in agreement with optical microscopy with polarized light (data not shown). The iPP dewetting occurs only in iPP-rich blends, and this phenomenon was used to discern if the morphology is caused by phase separation or iPP crystallization.

The morphology of phase behavior as a function of blend composition is shown in Fig. 6. Fig. 6(a) and (b) are the 90/10 and 5/95 iPP/PE blends annealed at 120 °C, respectively. Both of them show phase-separated droplets. As the composition is changed to 70/30 (Fig. 6(c)) and 30/70 (Fig. 6(d) iPP/PE annealed at 140 °C, once again, phase separation is observed. The droplets of the dispersed phase begin to coalesce. The 50/50 iPP/PE blend annealed at 145 °C (Fig. 6(e)) shows similar morphology, but the domain sizes of the two components are approximately equal and the phases appear to have coalesced more. The small droplets in the image are attributed to iPP spherulites. As the temperature increases to 160 °C (see Fig. 6(f)), which is above the melting temperature of two components, the surface is flat, and the blend becomes homogeneous.

In the two-phase region, as expected, the 50/50 composition shows the largest domain size. As the composition decreases from 50/50 on either side, the phase boundary also recedes. It is instructive to note that the ratio of the surface areas of the two components is approximately equal to the bulk volume fraction of the

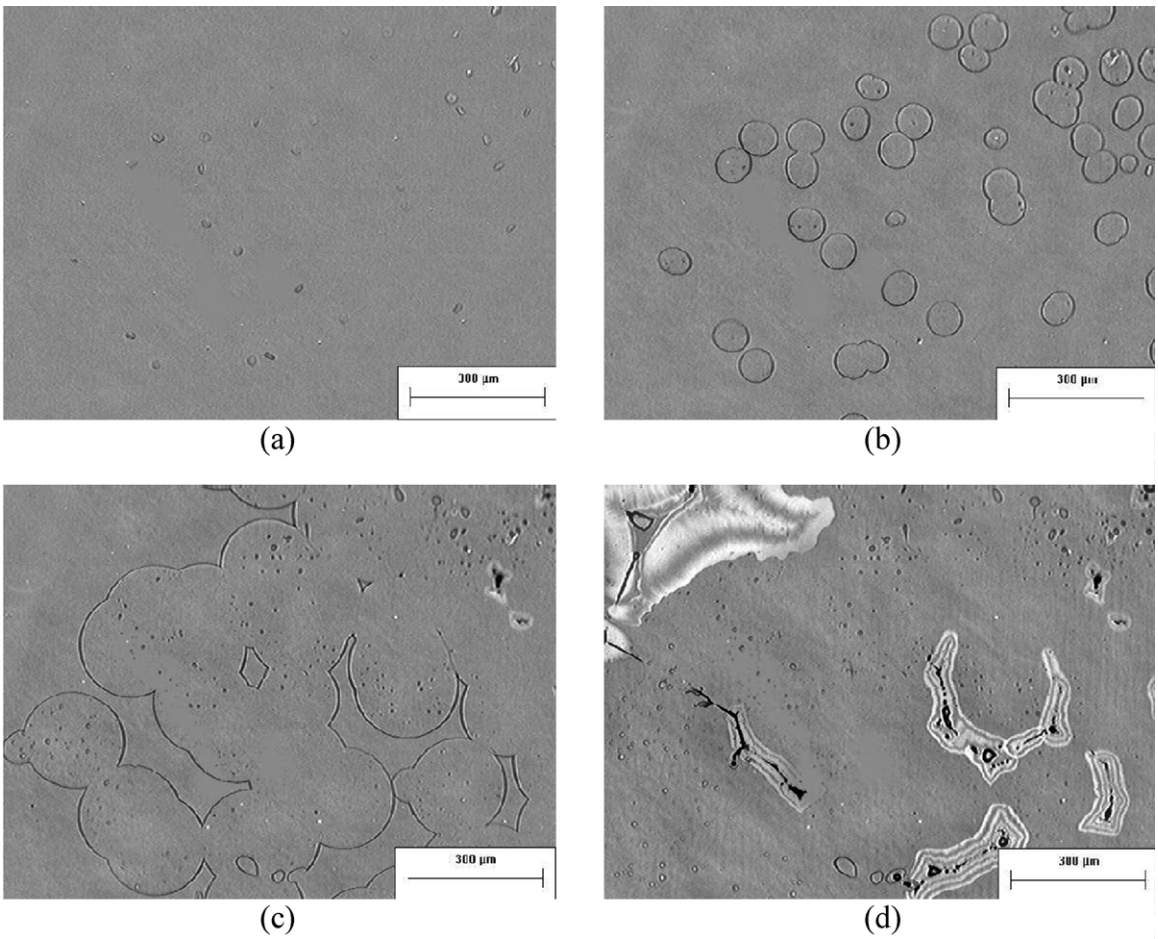

Fig. 5. The growth of iPP spherulites in iPP/PE (90/10 (v/v)) blends. The sample was annealed at 130 °C for: (a) 3 min, (b) 10 min, (c) 30 min, and (d) 180 min.

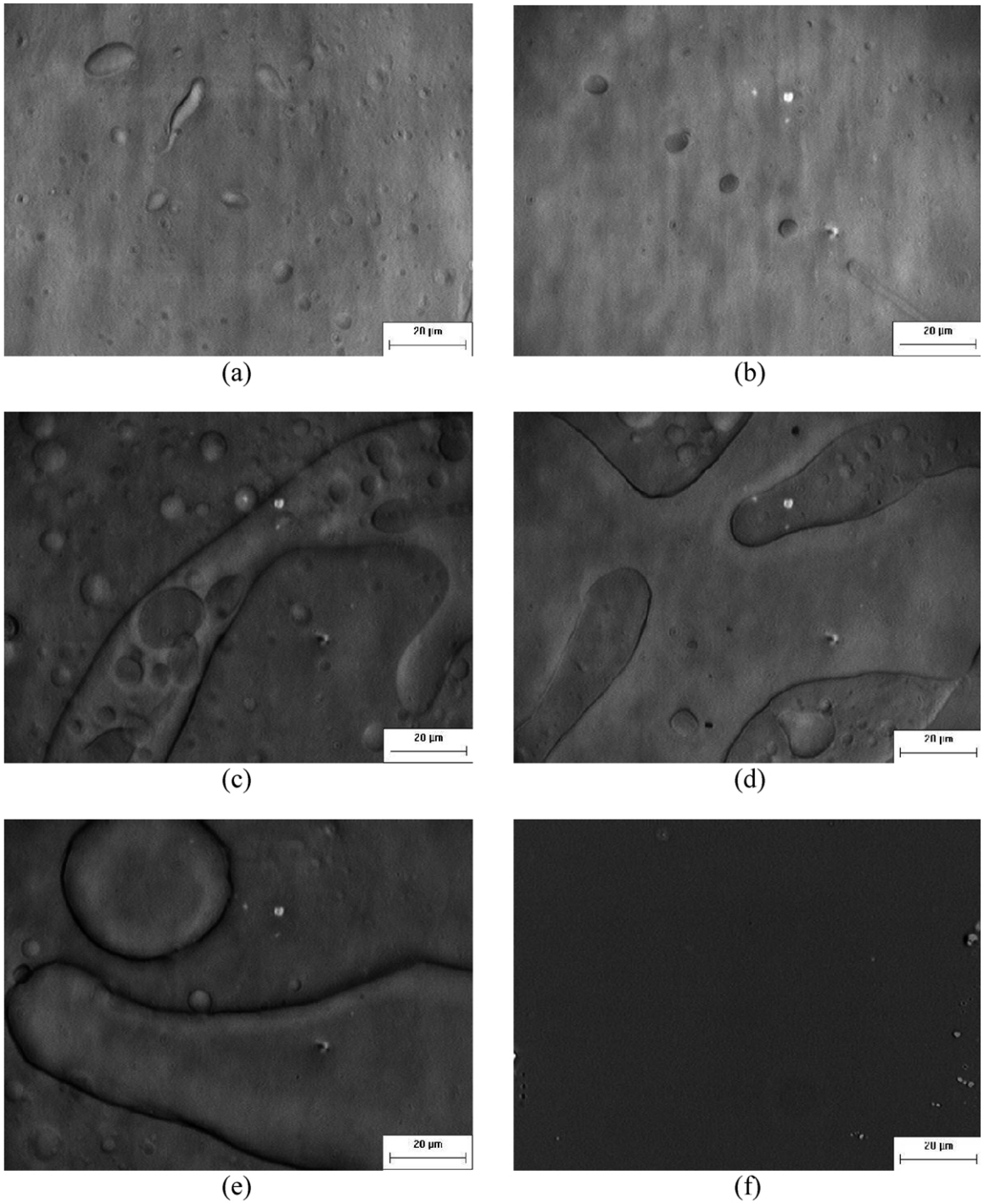

Fig. 6. Morphology of iPP/PE blends: (a) iPP/PE (90/10 (v/v)) annealed at 120 °C, (b) iPP/PE (5/95 (v/v)) annealed at 120 °C, (c) iPP/PE (70/30 (v/v)) annealed at 140 °C, (d) iPP/PE (30/70 (v/v)) annealed at 140 °C, (e) iPP/PE (50/50 (v/v)) annealed at 145 °C, (f) iPP/PE (50/50 (v/v)) annealed at 160 °C.

blend. In all of the images, the PE phase is higher than the iPP phase, since the surface energy of PE (90 mJ/m^2) [41] is higher than that of iPP (50–70 mJ/m^2) [42].

4. Conclusions

The temperature dependence of the iPP/PE interaction parameter χ was measured by SAXS. The phase diagram was predicted using Flory–Huggins theory and UCST behavior was exhibited with a critical temperature of 143 °C for the molecular weights used in this study. The comparison of χ between SAXS (this study) and SANS (on deuterium-labeled moieties) shows that the χ obtained from SANS is larger than SAXS due to the additional incompatibility caused by the presence of deuterium. In

addition, our data do not agree with the simple solubility parameter-based prediction of χ for unlabeled blends based on the χ for singly labeled blends.

The phase diagram was verified by optical microscopy. In optical microscopy, kinetics of phase separation and crystallization of iPP affect the observation of phase behavior. During iPP crystallization, the growth of iPP spherulites competes with the phase separation of the system in iPP-rich blends. In this case, dewetting caused by the iPP crystals provides a way to delineate phase separation and iPP spherulites.

The cloud points obtained from optical microscopy are consistent with the predicted phase diagram. This phase diagram is a first step towards understanding the role of the intermolecular interaction between iPP and PE on strengthening interfaces between these semicrystalline polymers.

Acknowledgements

The authors wish to acknowledge the financial support from the USDOE Ames Laboratory. This work also benefited from IPNS and the use of the SAXS instrument at 12-ID at APS funded by the USDOE, BES under contract W-31-109-ENG-38 to the University of Chicago.

References

[1] Li J, Shanks RA, Long Y. J Appl Polym Sci 2001;82:628–39.
[2] Li J, Shanks RA, Olley RH, Greenway GR. Polymer 2001;42:7685–94.
[3] Li J, Shanks RA, Long Y. Polymer 2001;42:1941–51.
[4] Kukaleva N, Jollands M, Cser F, Kosior E. J Appl Polym Sci 2000;76:1011–8.
[5] Shanks RA, Li J, Yu L. Polymer 2000;41:2133–9.
[6] Greco R, Mucciariello G, Ragosta G, Martuscelli E. J Mater Sci 1980;15:845–53.
[7] Gross B, Peterman J. J Mater Sci 1984;19:105–12.
[8] Blom HP, Teh JW, Bremner T, Rudin A. Polymer 1998;39(17):4011–22.
[9] Martuscelli E, Pracella M, Avella M, Greco R. Makromolekulare Chemie 1980;181(4):957–67.
[10] Dong L, Olley RH, Bassett DC. J Mater Sci 1998;33:4043–8.
[11] Teh JW. J Appl Polym Sci 1983;28:605–18.
[12] Dumoulin MM, Carreau PJ, Utracki LA. Polym Engng Sci 1987;27(20):1627–33.
[13] Kukaleva N, Cser F, Jollands M, Kosior E. J Appl Polym Sci 2000;77:1591–9.
[14] Cser F, Rasoul F, Kosior E. Polym Engng Sci 1999;39(6):1100–8.
[15] Niebergall U, Bohse J, Seidler S, Grellmann W, Schurmann BL. Polym Engng Sci 1999;39(6):1109–18.
[16] Blom HP, Teh JW, Rudin A. J Appl Polym Sci 1996;61:959–68.
[17] Varin RA, Djokovic D. Polym Engng Sci 1988;29(22):1477–83.
[18] Li J, Shanks RA, Long Y. J Appl Polym Sci 2000;76:1151–64.
[19] Flory PJ. Principles of polymer chemistry. Ithaca, NY: Cornell University Press; 1953.
[20] Koningsveld R, Staverman J. J Polym Sci, Polym Phys Ed 1968;6:305–23.
[21] Koningsveld R, Kleintjens LA, Shultz AR. J Polym Sci, Polym Phys Ed 1970;8:1261–78.
[22] Lin CC, Jonnalagadda SV, Balsara NP, Han CC, Krishnamoorti R. Macromolecules 1996;29:661–9.
[23] Freed KF, Dudowicz J. Macromolecules 1996;29:625–36.
[24] Jeon HS, Lee JH, Balsara NP. Macromolecules 1998;31:3328–39.
[25] Jeon HS, Lee JH, Balsara NP, Newstein MC. Macromolecules 1998;31:3340–52.
[26] Wang H, Wang GZG, Han CC, Hsiao BS. Polym Mater Sci Engng 2001;85:427–8.
[27] Rhee J, Crist B. J Chem Phys 1993;98(5):4174–82.
[28] Graessley WW, Krishnamoorti R, Balsara NP, Fetters LJ, Lohse DJ, Schulz DN, Sissano JA. Macromolecules 1993;26:1137–43.
[29] Rajasekaran JJ, Curro JG, Honetcutt JD. Macromolecules 1995;28:6843–53.
[30] Singh C, Schweizer KS. J Chem Phys 1995;103(13):5814–32.
[31] Fredrickson GH, Liu AJ, Bates FS. Macromolecules 1994;27:2503–11.
[32] Gromov DG, de Pablo JJ. J Chem Phys 1998;109(22):10042–52.
[33] Koch T, Strobl GR. J Polym Sci, Polym Phys Ed 1990;28:343–53.
[34] Roe RJ. Methods of X-ray and neutron scattering in polymer science. New York: Oxford University Press; 2000.
[35] Cebe P, Hsiao BS, Lohse DJ. Scattering from polymers: characterization by X-rays neutrons, and light. ACS Symposium Series, vol. 739. Washington, DC: American Chemical Society; 2000.
[36] de Gennes PG, Scaling concepts in polymer physics, Ithaca, NY: Cornell University Press; 1979.
[37] Strobl GR. The physics of polymers: concepts for understanding their structures and behavior, 2nd ed. Berlin: Springer; 1997.
[38] Sperling LH. Introduction to physical polymer science, 3rd ed. New York: Wiley-Interscience; 2001.
[39] Zirkel A, Urban V, Richter D, Fetters LJ, Huang JS, Kampmann R, Hadjichristidis N. Macromolecules 1992;25:6148–55.
[40] Boothroyd AT, Rennie AR, Boothroyd CB. Europhys Lett 1991;15(7):715–9.
[41] Crist B, Mirabella FM. J Polym Sci, Polym Phys Ed 1999;37:3131–40.
[42] Cheng SZD, Janimak JJ, Zhang A, Hsieh ET. Polymer 1991;32(4):648–55.